Lane formation and critical coarsening in a toy model of bacterial competition

Takuro Shimaya* and Kazumasa A. Takeuchi†

Department of Physics, Tokyo Institute of Technology,
2-12-1 Ookayama, Meguro-ku, Tokyo, 152-8551, Japan

(Dated: September 4, 2022)

We study competition of two non-motile bacterial strains in a three-dimensional channel numerically, and analyze how their configuration evolves in space and time. We construct a lattice model that takes into account self-replication, mutation, and killing of bacteria. When mutation is not significant, the two strains segregate and form stripe patterns along the channel. The formed lanes are gradually rearranged, with increasing length scales in the two-dimensional cross-sectional plane. We characterize it in terms of coarsening and phase ordering in statistical physics. In particular, for the simple model without mutation and killing, we find logarithmically slow coarsening, which is characteristic of the two-dimensional voter model. With mutation and killing, we find a phase transition from a monopolistic phase, in which lanes are formed and coarsened until the system is eventually dominated by one of the two strains, to an equally mixed and disordered phase without lane structure. The logarithmic coarsening is found at the transition point, which can be understood as a realization of the generalized voter universality class for absorbing-state transitions. These results are accounted for by continuum equations, obtained by applying a mean field approximation along the channel axis. Our findings suggest relevance of critical coarsening and absorbing-state transitions in the context of bacterial competition.

arXiv:1804.09895v2 [q-bio.PE] 1 May 2018

Introduction – Competition and evolution of multiple biological species, such as those in ecosystems, constitute one of the key situations where ideas of statistical physics can contribute to quantitative understanding of biological problems and vice versa [1–4]. Traditionally, theoretical approaches to such competition processes often assumed uniform systems without any spatial structure [1, 5], which correspond to studying well-mixed populations. However, recent experiments have shown that, when multiple strains of bacteria are cultured on agar plates (or on agarose surfaces), nontrivial domain structures are formed, which then interplay with their population and evolutionary dynamics [6–10]. Formation of clonal domains, as well as their spatiotemporal evolution, were also observed in stem cell tissues, and shed light on mechanisms of homeostasis [11, 12]. Also backed by a surge of theoretical interests in evolutionary dynamics [3, 4] and active matter [13], interplay between competition and spatial degrees of freedom has aroused increasing attention.

Recent experimental developments on microfluidic devices [14] add another aspect to this problem. An advantage of microfluidic systems is that one has control over various experimental conditions, such as cell environments and the system geometry. Indeed, it is now clear that the system geometry can have a crucial impact on collective properties of cells [15, 16]. One of the common geometries for long time measurement is a channel with open ends, such as the mother machine [17], used to characterize growth and division of single cells, cell lineage, statistical properties of cell populations, etc. [17–22]. As such, it is also a natural geometry to use for studying competition problems.

Here we study, on the basis of a simple model, competition of two non-motile bacterial strains in a channel with open ends. The two strains are differently labeled but otherwise isogenic. In its simplest version, the model consists of self-replication of cells, volume exclusion, and escape from the open ends. Then we find that initially mixed populations spontaneously segregate, forming lane structures along the channel. Spatiotemporal evolution of lanes can be characterized in terms of phase ordering in the two-dimensional cross section of the channel. Remarkably, it turns out to show logarithmically slow coarsening, characteristic of the two-dimensional voter model [23, 24]. We also generalize the model by introducing mutation and killing of bacteria, and find a transition from a monopolistic phase, in which lanes are formed and coarsened until the system is eventually dominated by one of the two strains, to an equally mixed and disordered phase without lane structure. Interestingly, the voter-type coarsening corresponds to the critical point between those two phases. These results are accounted for by continuum equations, which we obtain by the mean field approximation along the channel axis.

Model with self-replication only – Let us start with the simplest model. Here we consider two strains of non-motile bacteria that self-replicate, inside an open channel with rectangular cross section (Fig. 1). The system is a three-dimensional lattice of size $L_x \times L_y \times L_z$. The x-axis is taken along the channel. We impose the open boundary condition at the channel ends and the periodic one at the walls. Each site is occupied by a cell of genotype $s(x, y, z, t) \in \{-1, 1\}$ (shown in yellow and purple, respectively, in Fig. 1). Each cell has a division age $\tau_{\rm rep}$. Following an experimental observation of *Es-*

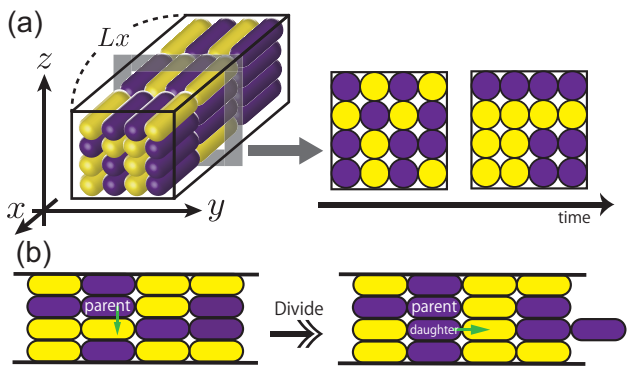

FIG. 1. Illustration of the model with self-replication only. (a) Sketch of the system. The channel is along the x-axis and filled with two strains of bacteria (yellow and purple). If lanes are formed along the channel, their arrangement can be characterized by cross sections. (b) Sketch of the time evolution rule. When a cell (marked "parent") divides, a daughter cell of the same genotype is generated randomly at one of the six neighboring sites (see text). The cell that previously occupied the target site is then pushed in either direction along the channel, again chosen randomly. This expels a cell from the channel, which is simply removed from the system.

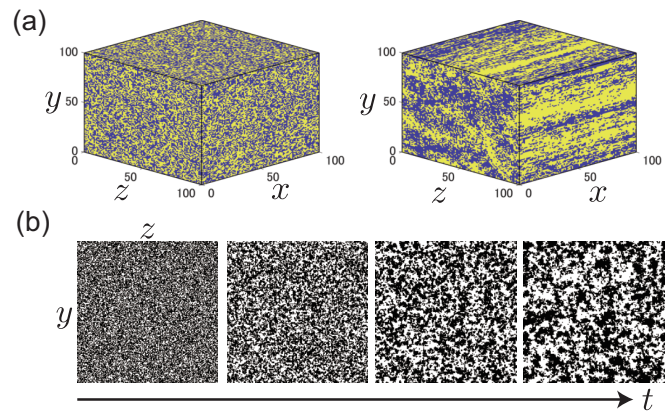

FIG. 2. Lane formation and subsequent coarsening in the model with self-replication only. (a) Three-dimensional view of the system. The two strains are indicated by yellow ($s = -1$) and purple ($s = +1$). The left and right figures show the configuration at different times, $t = 0$ (initial condition) and $t = 50000$, respectively. The system size is $L_x = L_y = L_z = 100$. See also Movie S1 [27]. (b) Time evolution of the two-dimensional magnetization field $\phi(y, z, t)$ (■:$\phi > 0$, □:$\phi \leq 0$) at $t = 0, 300, 1500, 5000$ from left to right. The system size is $L_x = L_y = L_z = 200$. See also Movie S2 [27].

cherichia coli [21], here we assume the gamma distribution for $\tau_{\rm rep}$ [25]. When the division time comes, the cell generates a daughter with the same genotype s at one of the six nearest-neighbor sites. This neighbor is chosen as follows: first the direction is chosen to be longitudinal or transverse, with respect to the channel axis, then one of the neighbors is selected at equal probability. As a result, neighbors in the x direction are chosen at probability 1/4 and those in the yz direction at 1/8. Figure 1(b) illustrates an example in which the replication takes place in a direction perpendicular to the channel walls. In this case, the generated daughter cell pushes the existing cell toward either end of the channel, which is again chosen randomly. The row of cells is pushed thereby, and the one at the extremity is expelled from the system. The total number of the cells is therefore conserved. If the replication occurs along the channel, the row of cells is pushed similarly. Both of the divided cells renew their $\tau_{\rm rep}$ according to the gamma distribution. In the following, we fix the parameters of the gamma distribution so that the mean is $\mathrm{E}[\tau_{\rm rep}] = 50$ and the variance is $\mathrm{Var}[\tau_{\rm rep}] = 200$. Simulations were carried out by using Gillespie's algorithm [26] with continuous time.

Figure 2(a) and Movie S1 [27] show time evolution of the system from a random initial condition. We find that the two, initially mixed strains of bacteria segregate in the course of time, forming lanes along the channel. Moreover, typical width of those lanes grows with time (see the movie). This suggests the relevance of coarsening and dynamic scaling in statistical physics [28], which describes, e.g., how the domains of up and down spins evolve in the ferromagnetic phase of the Ising model. There is an obvious analogy because our variable s is also dichotomous, but the time evolution of our model does not satisfy the detailed balance (in this sense non-equilibrium) and is anisotropic by construction.

To characterize the observed anisotropic coarsening, we introduce the following local "magnetization"

$$\phi(y, z, t) := \frac{1}{L_x} \sum_{x}^{L_x} s(x, y, z, t), \tag{1}$$

which is a function of cross-sectional coordinates (y, z) and time. The sign of $\phi(y, z, t)$, denoted by $\mathrm{sign}[\phi(y, z, t)]$, indicates the strain that takes the majority in each line along the channel. Figure 2(b) shows space-time evolution of $\mathrm{sign}[\phi(y, z, t)]$. This clearly shows the growth of length scales – an important characteristic of coarsening processes – in cross sections. On the other hand, the intricate structure of the observed patterns does not seem to be characterized by a single growing length scale; as a matter of fact, the domain interfaces are irregular down to the smallest length scale of the system, i.e., the lattice constant. It is contrasted with coarsening in the ferromagnetic Ising model and that of other curvature-driven interfaces, for which interfaces are smoothed by effective surface tension [28].

One of the standard method for characterizing coarsening is to measure the total length of the domain interfaces. For our model, we use $\mathrm{sign}[\phi(y, z, t)]$ to determine the domains, and measure the interface density $\rho(t)$, defined by the fraction of site pairs with the opposite signs [Fig. 3(a)]. In contrast to usual curvature-driven coarsening, for which $\rho(t)$ typically decays by a power law [28],

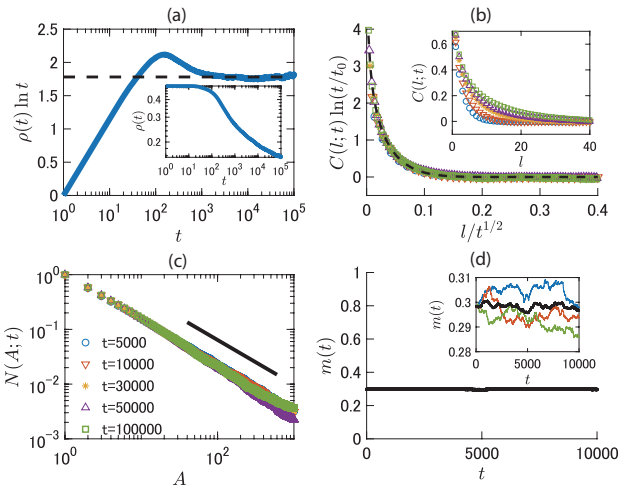

FIG. 3. Results for the model with self-replication only, averaged over 10 independent realizations. The system size is $L_x = L_y = L_z = 300$. (a) The interface density in the ϕ-field, $\rho(t)$. $\rho(t)\ln t$ is plotted in the main panel, while the raw data is shown in the inset in the log-log chart (see also Fig. S1). The horizontal dashed line is a guide for the eyes, showing logarithmic decay of the data, $\rho(t) \sim 1/\ln t$. (b) The spatial correlation function $C(l;t)$ at $t = 5000(\circ), 10000(\triangledown), 30000(*), 50000(\triangle), 100000(\square)$ (from lower left to upper right in the inset). $t_0 = 300$ is used. The black dashed line shows the Ei function fitted to the data at $t = 100000$. The inset shows the raw data without rescaling. (c) The cumulative distribution of domain size A, $N(A;t)$. The solid line is a guide for the eyes indicating our estimate of the exponent value $\tau = 0.81(3)$. (d) The total magnetization $m(t)$, for simulations with biased initial conditions $m(0) \approx 0.3$. The black bold line shows the ensemble average over 10 realizations, zoomed in the inset, and the thinner color lines in the inset show individual time series. The data in (a)-(c) are obtained with unbiased initial conditions $m(0) \approx 0$.

here $\rho(t)$ seems to decay more slowly (inset and Fig. S1 [27]). Indeed, if $\rho(t)\ln t$ is plotted instead (main panel), we find an extended plateau asymptotically, which indicates $\rho(t) \sim 1/\ln t$. In fact, this logarithmic decay is known to be characteristic of the two-dimensional voter model [23, 24], a simple model for opinion formation. Similarity to the voter model is also apparent from the evolution of sign$[\phi(y,z,t)]$ [Fig. 2(b)], which resembles that of the voter model [23, 24]. These results are robust against changes in the system aspect ratio, as we checked for both elongated ($L_x > L_y = L_z$) and shortened ($L_x < L_y = L_z$) channels (Fig. S2).

The appearance of the characteristic coarsening of the voter model is further confirmed quantitatively. For example, the largest length scale of the pattern is known to grow as $t^{1/2}$ in the voter model [23, 24, 29]. A way to see this is to measure the spatial correlation function

$$C(l;t) := \langle \phi(\boldsymbol{r}+\boldsymbol{l},t)\phi(\boldsymbol{r},t)\rangle - \langle \phi(\boldsymbol{r},t)\rangle^2 , \qquad (2)$$

with $\boldsymbol{r} := (y,z)$ and $l := |\boldsymbol{l}|$. The tail of the measured correlation function is indeed more extended for larger times [Fig. 3(b) inset], showing growth of the relevant length scale. For the voter model, the asymptotic expression of the correlation function is known to be [30, 31]

$$C(l;t) \simeq \frac{\mathrm{Ei}_1(l^2/2t)}{\ln(t/t_0)}, \qquad (3)$$

with the exponential integral (Ei) function $\mathrm{Ei}_1(\xi) := \int_\xi^\infty w^{-1}e^{-w}\mathrm{d}w$ and a microscopic time scale t_0, which is 1/16 for the voter model but is in general a model-dependent quantity. This form of rescaling is tested in Fig. 3(b) main panel. The data are found to overlap very well, being in remarkable agreement with the Ei function predicted for the voter model (dashed line). We also measure the cumulative distribution of the domain area A at time t, $N(A;t)$ [Fig. 3(c)]. As opposed to the correlation function, the domain area distribution is governed by different length scales that coexist in the pattern, and as a result it is essentially independent of time. We find a power-law distribution $N(A;t) \sim A^{-\tau}$, which implies fractal structure of the pattern. We obtained an exponent value $\tau = 0.81(3)$ from the data at $t = 100000$, which is consistent with a past study on the voter model [23]. Agreement with the voter model is also seen in statistical properties of the change of sign$[\phi(y,z,t)]$, such as the persistence probability $P_0(t)$ and the average number of sign flips $\langle n(t)\rangle$ (Fig. S3), studied numerically for the voter model in [32]. Finally, we also measure the total magnetization of the system, $m(t) := \langle s(x,y,z,t)\rangle$, and find that it remains statistically constant, even if we start from a biased initial condition [Fig. 3(d)]. Statistical conservation of m is also an important characteristic of the voter model [24].

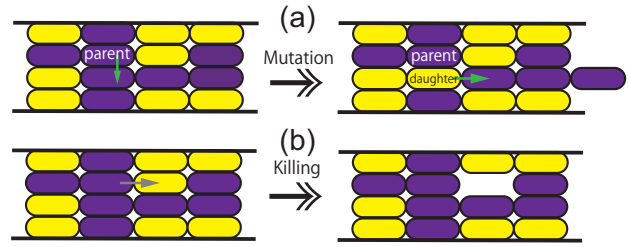

FIG. 4. Mutation and killing considered in the extended model. (a) Mutation. When a cell replicates, the daughter's genotype becomes different from that of the parent at probability p_m. (b) Killing. A cell chooses a neighbor to attack randomly. If the genotype of the attacked cell is different from that of the killer, the attacked one is killed and leaves a void. It is a stochastic event that occurs independently from replications.

Model with mutation and killing – To investigate the robustness of our results under more general situations, we extend our model by including mutation and killing of bacteria (Fig. 4). For simplicity, here the mutation is implemented by an event in which a parent cell gener-

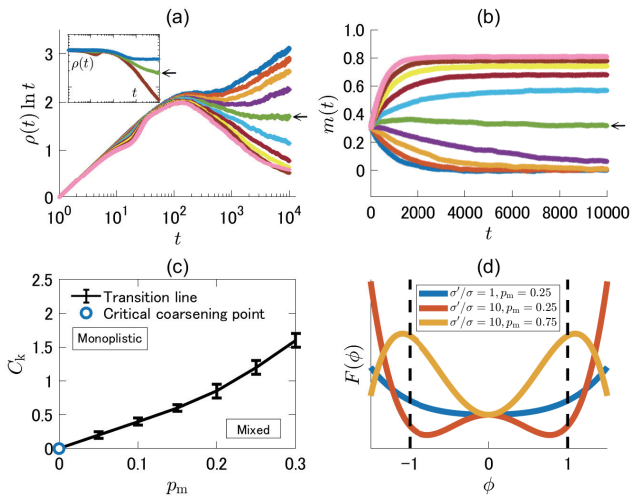

FIG. 5. Results for the model with mutation and killing. Numerical results were obtained with system size $L_x = 100$ and $L_y = L_z = 200$, each data set taken from a single realization. (a,b) The interface density $\rho(t)$ (a) and the total magnetization $m(t)$ (b) for different C_k with p_m fixed at 0.05. C_k is varied from 0 to 0.45 [from top to bottom for (a), from bottom to top for (b)]. Here the biased initial conditions, $m(0) \approx 0.3$, are used. The green curve indicated by the arrow ($C_\mathrm{k} = 0.2$) is considered to be closest to the transition point. (c) Phase diagram in the $(p_\mathrm{m}, C_\mathrm{k})$ plane. (d) Profile of the free energy density $F(\phi)$ [Eq. (S23)] in the obtained continuum equations.

ates a daughter with the genotype s, or allele, opposite to that of the parent [Fig. 4(a)]. We assume that such a mutation occurs at probability p_m in each replication. For the killing, we implement it by the following stochastic event, having in mind the bacterial type VI secretion system (T6SS) [10, 33, 34]. When a cell decides to kill, it chooses a target randomly among the neighbors. If and only if the chosen cell has the genotype different from the killer's, it is killed and a void is generated. This void, encoded as $s = 0$, can be taken by a cell generated at a later time. A killing event occurs randomly and independently from replications. The waiting time, τ_kill, is generated from the exponential distribution with mean $\mathrm{E}[\tau_\mathrm{kill}]$. We define a parameter $C_\mathrm{k} := \mathrm{E}[\tau_\mathrm{rep}]/\mathrm{E}[\tau_\mathrm{kill}]$. The previous model without mutation and killing corresponds to taking $p_\mathrm{m} = 0$ and $C_\mathrm{k} = 0$.

Carrying out simulations for various values of p_m and C_k, we find that lane formation and subsequent coarsening occur as well, for relatively small p_m or large C_k. Figure 5(a) inset and Fig. 5(b) show the density of interfaces in $\mathrm{sign}[\phi(y,z,t)]$, $\rho(t)$, and the total magnetization $m(t)$, respectively, for $p_\mathrm{m} = 0.05$ and C_k varied from 0 to 0.45. For large C_k, we observe lane formation and coarsening (Fig. S4 and Movie S3 [27]), accompanied by decrease of $\rho(t)$ [Fig. 5(a) inset]. However, unlike the voter-type coarsening in the previous model, the interfaces are smoother (Fig. S4), $\rho(t)$ decreases faster than $1/\ln t$ [Fig. 5(a) main panel, lower curves], and $m(t)$ is not conserved but takes a non-zero asymptotic value determined by the choice of the parameter values [Fig. 5(b) upper curves]. This means that the system is eventually dominated by one of the two strains. In contrast, if C_k is small, lanes are not formed (Fig. S5 and Movie S4), $\rho(t)$ stops decreasing [Fig. 5(a) inset top curve], and $m(t)$ vanishes [Fig. 5(b) lower curves]. In other words, the two strains remain mixed and equally populated. Figure 5(c) shows a phase diagram in the $(p_\mathrm{m}, C_\mathrm{k})$ plane, where the monopolistic (ordered) and mixed (disordered) phases are bordered by a transition line. At the transition, our data suggest that $\rho(t) \sim 1/\ln t$ and $m(t)$ remains roughly constant [Fig. 5(a,b), green curves indicated by the arrows]. Therefore, the voter-type coarsening seems to appear at the transition point. In particular, the simpler case without mutation and killing, $(p_\mathrm{m}, C_\mathrm{k}) = (0, 0)$, corresponds to the endpoint of the transition line [Fig. 5(c)].

These results can be interpreted as follows. First of all, while mutation obviously makes the configuration more disordered, killing actually plays a role analogous to the Ising ferromagnetic interaction. This is because, firstly, killing occurs only between cells of different genotypes, and secondly, the void left by the killed cell is eventually taken by a daughter from one of the neighbors. As a result of these competing effects, the ordered and disordered phases appear, similarly to the ferromagnetic Ising model. Moreover, the presence of the Ising-like ferromagnetic interaction also implies that the interfaces are now endowed with effective surface tension [28], which can explain why those in the ordered phase are smoother than the voter-type coarsening observed at the transition.

Finally, it is known that the characteristic coarsening of the voter model actually represents a broad class of phase transitions into absorbing states [35] in the presence of the Ising-like up/down symmetry, called the (generalized) voter universality class [24, 36]. Systems in the voter class usually have two symmetric absorbing states, labeled by "spin" variable $+1$ and -1. The defining feature of those absorbing states is that bulk nucleation of the opposite spin is forbidden; in other words, once the spin variables become globally $+1$ or -1, this uniform configuration is kept forever. Such systems can show two different phase transitions, one for spontaneous symmetry breaking of magnetization, and the other for whether the system eventually falls into one of the two absorbing states. According to the established scenario [36], if these transitions occur separately, the former is in the Ising class and the latter is in the directed percolation class. However, the two transitions can also occur simultaneously in generic models, and in this case the voter universality class arises. In our model, such symmetric absorbing states indeed exist in the case without mutation, and at the transition the voter-class behavior is clearly observed. An interesting observation is that, in the presence of mutation, such strict absorbing states do

not exist anymore, as we can see from the fact that the magnetization in the ordered phase is not ± 1 [Fig. 5(b)]. Nevertheless, after the lane formation, each line along the channel is dominated by either strain, and the majority rarely changes if the channel length is long enough. Therefore, the transition is still effectively an absorbing state transition under the up/down symmetry, and the voter universality class follows.

Theory – The numerical results presented so far can be understood by means of continuum equations, which we obtain in the following by a mean-field-like approximation. The variable to use is the local magnetization field $\phi(\boldsymbol{r}, t)$ with $\boldsymbol{r} = (y, z)$ in the cross-sectional plane. Suppose, at position $\boldsymbol{r}_i$, $\phi_i := \phi(\boldsymbol{r}_i, t)$ changes by $\Delta\phi_i$ during a small time step Δt. $\Delta\phi_i$ can be expressed as follows,

$$\Delta\phi_i = \Delta\phi_{i\to i} + \sum_{j\in\{\text{n.n of i}\}} \Delta\phi_{j\to i}, \tag{4}$$

where n.n. refers to the nearest neighbors in the yz plane, and $\Delta\phi_{j\to i}$ denotes the contribution from the line $\boldsymbol{r}_j$ to $\boldsymbol{r}_i$. The change $\Delta\phi_{j\to i}$ results from replications, mutations, and killing events that occur locally and independently between the two lines. Therefore, by the central limit theorem, it can be approximated by

$$\Delta\phi_{j\to i} = \mathrm{E}[\Delta\phi_{j\to i}] + \sqrt{\mathrm{Var}[\Delta\phi_{j\to i}]}\epsilon_{j\to i}(t), \tag{5}$$

where $\epsilon_{j\to i}(t)$ is white Gaussian noise with $\langle\epsilon_{j\to i}\rangle = 0$ and $\langle\epsilon_{j\to i}(t)\epsilon_{j'\to i'}(t')\rangle = \delta_{ii'}\delta_{jj'}\delta_{tt'}$.

The mean $\mathrm{E}[\Delta\phi_{j\to i}]$ and the variance $\mathrm{Var}[\Delta\phi_{j\to i}]$ can be evaluated by considering, for each type of events, the Poisson distribution for the number of the events and the probability that such an event changes the magnetization ϕ_i, within the mean-field approximation (see Supplemental Text [27]). For simplicity, here we consider that replications and killing attempts occur at constant rates σ and σ', respectively (roughly $\sigma \approx 1/\mathrm{E}[\tau_{\mathrm{rep}}]$ and $\sigma' \approx 1/\mathrm{E}[\tau_{\mathrm{kill}}]$), and the void generated by killing is filled immediately by replication from a neighboring site. Then, taking the limit $\Delta t \to 0$ and coarse-graining in space, we obtain

$$\begin{aligned}\frac{\partial\phi(\boldsymbol{r},t)}{\partial t} =& -\frac{\delta F(\phi)}{\delta\phi} + A_1\nabla^2\phi \\ &+ \sqrt{A_2(1-\phi^2) + A_3\phi^2}\ \eta(\boldsymbol{r},t)\end{aligned} \tag{6}$$

with a Landau-like free energy density

$$F(\phi) = A_4\phi^2 + A_5\phi^4 \tag{7}$$

and coefficients

$$\begin{aligned} A_1 &= a^2\left[\frac{\sigma}{8}(1-p_{\mathrm{m}}) + \frac{\sigma'}{16}\right], \\ A_2 &= \frac{a^2}{L_x}(\sigma + 2\sigma'), & A_3 &= \frac{2a^2}{L_x}\sigma p_{\mathrm{m}}, \\ A_4 &= -\left(\frac{1-2p_{\mathrm{m}}}{4}\sigma' - p_{\mathrm{m}}\sigma\right), & A_5 &= \frac{1-2p_{\mathrm{m}}}{8}\sigma'. \end{aligned} \tag{8}$$

Here, $\eta(\boldsymbol{r}, t)$ is white Gaussian noise with $\langle\eta(\boldsymbol{r}, t)\rangle = 0$ and $\langle\eta(\boldsymbol{r}, t)\eta(\boldsymbol{r}', t')\rangle = \delta(\boldsymbol{r}' - \boldsymbol{r})\delta(t - t')$, and a is the lattice constant.

Several remarks are now in order. First, in the case without mutation and killing ($p_{\mathrm{m}} = \sigma' = 0$), we have $A_1, A_2 > 0$ and $A_3 = A_4 = A_5 = 0$. Then Eq. (S22) becomes the Lengevin description of the voter model [37, 38], which underpins our observation of the voter-type coarsening in this case (Fig. 3). Second, though both coefficients of $F(\phi)$ can change the sign in general [Fig.5(d)], for $p_{\mathrm{m}} < 1/2$, A_5 remains positive, while A_4 changes the sign at $p_m = \frac{\sigma'}{4\sigma+2\sigma'} \approx \frac{C_{\mathrm{k}}}{4+2C_{\mathrm{k}}}$. This underlies the transition observed in Fig.5(c). Finally, since $-\frac{\delta F(\phi)}{\delta\phi} = \left[\frac{1-2p_{\mathrm{m}}}{2}\sigma'(1-\phi^2) - 2p_{\mathrm{m}}\sigma\right]\phi$, in the absence of mutation ($p_{\mathrm{m}} = 0$), the completely monopolistic situations $\phi(\boldsymbol{r}, t) = \pm 1$ correspond to the two absorbing states of Eq. (S22). Further, Eq. (S22) in this case takes the form of the continuum equation proposed by Al Hammal *et al.* for the generalized voter universality class [36]. If $p_{\mathrm{m}} \neq 0$, strictly, $\phi(\boldsymbol{r}, t) = \pm 1$ are not absorbing any more, but our numerical results in Fig.5(c) still seem to indicate the generalized voter class as we already discussed. In contrast, in the monopolistic (ordered) phase, the ordering process seems to be driven by curvature, or effective surface tension between the two domains (Fig. S4). This is indeed what is predicted for a continuum equation akin to ours [39]. However, while theoretically $\rho(t) \sim t^{-1/2}$ is expected in this case, in our simulations $\rho(t)$ decays significantly more slowly (Fig. S6). This apparent discrepancy, which may be due to an approximation made to derive the continuum equation, needs to be elucidated.

Summary - In this work, we constructed a toy model of competition between two strains of non-motile bacteria in a channel, driven by replication and killing of bacteria. In the simplest situation driven only by self-replications, we numerically found that the two strains segregate and form lane structures along the channel. The lanes then gradually thicken. This process was characterized in the cross-sectional plane and turned out to be governed by the coarsening process of the two-dimensional voter model. In the presence of killing and mutation, we revealed a transition between the mixed phase and the monopolistic phase. The transition is characterized by critical behavior of the generalized voter class, which includes the self-replication-only case at the end of the transition line. In the mixed phase, lane formation does not occur and the two strains are well-mixed, with equal proportion on average. In contrast, in the monopolistic case, one of the two strains dominates, though a coarsening process qualitatively similar to that of the Ising ferromagnet. Those findings were accounted for by a continuum equation we derived, based on the mean-field approximation along the channel.

We should note that, at the price of access to large-scale statistical properties, our model assumes an ideal-

ized situation, which in many aspects oversimplifies actual bacterial competition and ecosystems. In particular, we assumed that the mutation is reciprocal, switching always from a strain to the other. That is obviously unrealistic, but we believe this effect is negligible if the mutation rate is low enough and back mutation is rare. Of course, it is of crucial importance to test, in real experiments and/or more realistic models, nontrivial dynamics and statistical properties suggested by our model.

Acknowledgments - We acknowledge discussions with R. A. L. Almeida, H. Chaté, and I. Dornic. We thank Y. T. Fukai for having drawn our attention to [10], and T. P. Shimizu for a help in program coding. This work is supported in part by KAKENHI from Japan Society for the Promotion of Science (No. JP25103004, JP16H04033, JP16K13846) and by the grants associated with "Planting Seeds for Research" Program and Suematsu Award of Tokyo Tech.

* t.shimaya@noneq.phys.titech.ac.jp
† kat@kaztake.org

[1] J. F. Crow and M. Kimura, *An introduction to population genetics theory* (Harper and Row, New York, 1970).
[2] B. Drossel, *Advances in Physics*, Adv. Phys. **50**, 209 (2001).
[3] K. S. Korolev, M. Avlund, O. Hallatschek, and D. R. Nelson, Rev. Mod. Phys. **82**, 1691 (2010).
[4] See, e.g., special issue on Statistical Mechanics and the Dynamics of Evolution in J. Stat. Mech. (**2013**), Issue 01.
[5] P. Turchin, *Complex Population Dynamics: A Theoretical/Empirical Synthesis*, Monographs in Population Biology, Vol. 35 (Princeton Univ. Press, Princeton, 2003).
[6] O. Hallatschek, P. Hersen, S. Ramanathan, and D. R. Nelson, Proc. Natl. Acad. Sci. U. S. A. **104**, 19926 (2007).
[7] T. J. Rudge, F. Federici, P. J. Steiner, A. Kan, and J. Haseloff, *ACS Synthetic Biology*, ACS Synth. Biol. **2**, 705 (2013).
[8] D. P. Lloyd and R. J. Allen, J. R. Soc. Interface **12**, 20150608 (2015).
[9] F. D. Farrell, M. Gralka, O. Hallatschek, and B. Waclaw, J. R. Soc. Interface **14**, 20170073 (2017).
[10] L. Mcnally, E. Bernardy, J. Thomas, A. Kalziqi, J. Pentz, S. P. Brown, B. K. Hammer, P. J. Yunker, and W. C. Ratcliff, Nat. Commun. **8**, 14371 (2017).
[11] A. M. Klein and B. D. Simons, Development **138**, 3103 (2011).
[12] K. R. Mesa, K. Kawaguchi, D. G. Gonzalez, K. Cockburn, J. Boucher, T. Xin, A. M. Klein, and V. Greco, bioRxiv https://doi.org/10.1101/155408 (2017).
[13] M. C. Marchetti, J. F. Joanny, S. Ramaswamy, T. B. Liverpool, J. Prost, M. Rao, and R. A. Simha, Rev. Mod. Phys. **85**, 1143 (2013).
[14] G. Velve-Casquillas, M. L. Berre, M. Piel, and P. T. Tran, Nano Today **5**, 28 (2010).
[15] K. T. Wu, J. B. Hishamunda, D. T. Chen, S. J. DeCamp, Y. W. Chang, A. Fernández-Nieves, S. Fraden, and Z. Dogic, Science **355** (2017), 10.1126/science.aal1979.
[16] K. Beppu, Z. Izri, J. Gohya, K. Eto, M. Ichikawa, and Y. T. Maeda, Soft Matter **13**, 5038 (2017).
[17] P. Wang, L. Robert, J. Pelletier, W. L. Dang, F. Taddei, A. Wright, and S. Jun, Current Biology **20**, 1099 (2010).
[18] D. Volfson, S. Cookson, J. Hasty, and L. S. Tsimring, Proc. Natl. Acad. Sci. USA **105**, 15346 (2008).
[19] W. Mather, O. Mondragón-Palomino, T. Danino, J. Hasty, and L. S. Tsimring, Phy. Rev. Lett. **104**, 208101 (2010).
[20] Z. Long, E. Nugent, A. Javer, P. Cicuta, B. Sclavi, M. Cosentino Lagomarsino, and K. D. Dorfman, Lab on a chip **13**, 947 (2013).
[21] M. Hashimoto, T. Nozoe, H. Nakaoka, R. Okura, S. Akiyoshi, K. Kaneko, E. Kussell, and Y. Wakamoto, Proc. Natl. Acad. Sci. U. S. A. **113**, 3251 (2016).
[22] J. Sheats, B. Sclavi, M. Cosentino Lagomarsino, P. Cicuta, and K. D. Dorfman, R. Soc. open sci. **4**, 170463 (2017).
[23] M. Scheucher and H. Spohn, J. Stat. Phys. **53**, 279 (1988).
[24] I. Dornic, H. Chaté, J. Chave, and H. Hinrichsen, Phys. Rev. Lett. **87**, 045701 (2001).
[25] Iyer-Biswas *et al.* [40, 41] proposed the beta exponential distribution for the division time. In practice, however, with the coefficient of variation (standard deviation-to-mean ratio) of their experimental data, and within the range of the histogram they showed, the gamma distribution has a similar shape and therefore can be regarded as an approximate distribution.
[26] D. T. Gillespie, J. Phys. Chem. **81**, 2340 (1977).
[27] See Supplemental Material.
[28] A. J. Bray, Adv. Phys. **43**, 357 (1994), arXiv:cond-mat/9501089v1 http://arxiv.org/abs/cond-mat/9501089v1.
[29] J. Cox and D. Griffeath, The Annals of Probability **14**, 347 (1986).
[30] P. L. Krapivsky, Phys. Rev. A **45**, 1067 (1992).
[31] I. Dornic, Ph.D. thesis, Université de Nice, Sophia Antipolis (1998).
[32] E. BenNaim, L. Frachebourg, and P. L. Krapivsky, Phys. Rev. E **53**, 3078 (1996).
[33] B. T. Ho, T. G. Dong, and J. J. Mekalanos, Cell Host Microbe **15**, 9 (2014).
[34] A. B. Russell, S. B. Peterson, and J. D. Mougous, Nat. Rev. Microbiol **12**, 137 (2014).
[35] H. Hinrichsen, Adv. Phys. **49**, 815 (2000).
[36] O. Al Hammal, H. Chaté, I. Dornic, and M. A. Muñoz, Phys. Rev. Lett. **94**, 230601 (2005).
[37] R. Dickman and A. Y. Tretyakov, Phys. Rev. E **52**, 3218 (1995).
[38] M. A. Muñoz, G. Grinstein, and Y. Tu, Phys. Rev. E **56**, 5101 (1997).
[39] L. Dall'Asta and T. Galla, J. Phys. A **41**, 435003 (2008).
[40] S. Iyer-Biswas, G. E. Crooks, N. F. Scherer, and A. R. Dinner, Phys. Rev. Lett. **113**, 028101 (2014).
[41] S. Iyer-Biswas, C. S. Wright, J. T. Henry, K. Lo, S. Burov, Y. Lin, G. E. Crooks, S. Crosson, A. R. Dinner, and N. F. Scherer, Proc. Natl. Acad. Sci. USA **111**, 15912 (2014).

I. SUPPLEMENTAL TEXT : DERIVATION OF THE CONTINUUM EQUATION

We derive the continuum equation (6) in the main article, which describes the time evolution of the local magnetization $\phi(\boldsymbol{r},t)$ with corss-sectional coordinates $\boldsymbol{r}=(y,z)$, at coarse-grained scales. We start from Eqs. (4) and (5) for the lattice model:

$$\Delta\phi_i = \Delta\phi_{i\to i} + \sum_{j\in\{\text{n.n. of } i\}} \Delta\phi_{j\to i}, \tag{S1}$$

$$\Delta\phi_{j\to i} = \mathrm{E}[\Delta\phi_{j\to i}] + \sqrt{\mathrm{Var}[\Delta\phi_{j\to i}]}\epsilon_{j\to i}(t), \tag{S2}$$

where $\mathrm{E}[\cdot]$ and $\mathrm{Var}[\cdot]$ denote the mean and the variance, respectively, and $\epsilon_{j\to i}(t)$ is white Gaussian noise with $\langle\epsilon_{j\to i}(t)\rangle = 0$ and $\langle\epsilon_{j\to i}(t)\epsilon_{j'\to i'}(t')\rangle = \delta_{ii'}\delta_{jj'}\delta_{tt'}$. $\Delta\phi_{j\to i}$ is the variation of $\phi_i := \phi(\boldsymbol{r}_i,t)$ due to stochastic events that occur in a neighboring line $\boldsymbol{r}_j$, during a small time step Δt. Such a variation occurs, for example, when a cell at $\boldsymbol{r}_j$ replicates, produces its daughter at $\boldsymbol{r}_i$, and this repels a cell of the other strain (opposite spin) at either channel end. Similarly, ϕ_i varies when a cell at $\boldsymbol{r}_j$ kills a cell (of the different strain) at $\boldsymbol{r}_i$, and this void is filled by replication of a neighboring cell, which is assumed here to occur immediately for the sake of simplicity. Such series of events can occur only when the pair (or the triplet) of sites have appropriate combinations of the strain label s. The probability of having such combinations, $P^{\pm,\mathrm{rep}}_{j\to i}$ and $P^{\pm,\mathrm{kill}}_{j\to i}$, for replication and killing processes, respectively, with the double sign indicating whether ϕ_i increases or decreases, can be expressed as functions of ϕ's by employing a mean-field approximation. With those probabilities, as well as the number of replication events $\lambda_{\mathrm{rep}}(x,y,z)$ and that of killing events $\lambda_{\mathrm{kill}}(x,y,z)$ at a site (x,y,z) (with $\boldsymbol{r}_i=(y,z)$) during the time step Δt, $\Delta\phi_{j\to i}$ can be expressed as

$$\begin{aligned}\Delta\phi_{j\to i} =& \left(+\frac{2}{L_x}\right)\left\{\sum_{x}^{L_x P^{+,\mathrm{rep}}_{j\to i}} \lambda_{\mathrm{rep}}(x,y,z) + \sum_{x}^{L_x P^{+,\mathrm{kill}}_{j\to i}} \lambda_{\mathrm{kill}}(x,y,z)\right\} \\ &+ \left(-\frac{2}{L_x}\right)\left\{\sum_{x}^{L_x P^{-,\mathrm{rep}}_{j\to i}} \lambda_{\mathrm{rep}}(x,y,z) + \sum_{x}^{L_x P^{-,\mathrm{kill}}_{j\to i}} \lambda_{\mathrm{kill}}(x,y,z)\right\}.\end{aligned} \tag{S3}$$

Here, L_x is the channel length, or the total number of the cells in each lane.

Now, for simplicity, we assume that replication and killing events occur independently at constant rates σ ($\approx 1/\mathrm{E}[\tau_{\mathrm{rep}}]$) and σ' ($\approx 1/\mathrm{E}[\tau_{\mathrm{kill}}]$), respectively. Then the number of such events obey the Poisson distribution, so that $\mathrm{E}[\lambda_{\mathrm{rep}}(x,y,z)] = \mathrm{Var}[\lambda_{\mathrm{rep}}(x,y,z)] = \sigma\Delta t$ and $\mathrm{E}[\lambda_{\mathrm{kill}}(x,y,z)] = \mathrm{Var}[\lambda_{\mathrm{kill}}(x,y,z)] = \sigma'\Delta t$. We thereby obtain

$$\mathrm{E}[\Delta\phi_{j\to i}] = (+2)\left(\sigma\Delta t P^{+,\mathrm{rep}}_{j\to i} + \sigma'\Delta t P^{+,\mathrm{kill}}_{j\to i}\right) + (-2)\left(\sigma\Delta t P^{-,\mathrm{rep}}_{j\to i} + \sigma'\Delta t P^{-,\mathrm{kill}}_{j\to i}\right), \tag{S4}$$

$$\mathrm{Var}[\Delta\phi_{j\to i}] = \left(+\frac{2}{L_x}\right)^2\left(\sigma\Delta t L_x P^{+,\mathrm{rep}}_{j\to i} + \sigma'\Delta t L_x P^{+,\mathrm{kill}}_{j\to i}\right) + \left(-\frac{2}{L_x}\right)^2\left(\sigma\Delta t L_x P^{-,\mathrm{rep}}_{j\to i} + \sigma'\Delta t L_x P^{-,\mathrm{kill}}_{j\to i}\right). \tag{S5}$$

The probabilities $P^{\pm,\mathrm{rep}}_{j\to i}$ and $P^{\pm,\mathrm{kill}}_{j\to i}$ are evaluated by applying a mean-field approximation along each line of the channel. For the replication, with the effect of mutation taken into account, we obtain

$$P^{\pm,\mathrm{rep}}_{j\to i} = \frac{1}{8}(1-p_{\mathrm{m}})\frac{1\pm\phi_j}{2}\frac{1\mp\phi_i}{2} + \frac{1}{8}p_{\mathrm{m}}\frac{1\mp\phi_j}{2}\frac{1\mp\phi_i}{2} \qquad (j\neq i), \tag{S6}$$

$$P^{\pm,\mathrm{rep}}_{i\to i} = \frac{1}{2}(1-p_{\mathrm{m}})\frac{1\pm\phi_j}{2}\frac{1\mp\phi_i}{2} + \frac{1}{2}p_{\mathrm{m}}\frac{1\mp\phi_j}{2}\frac{1\mp\phi_i}{2}, \tag{S7}$$

where p_{m} is the probability that mutation occurs at each replication. Here, the factor $\frac{1\pm\phi_j}{2}$ corresponds to the probability that the cell to replicate at position $\boldsymbol{r}_j$ is the strain $s=\pm1$, and $\frac{1\pm\phi_i}{2}$ to the probability that the cell to be repelled from the channel at position $\boldsymbol{r}_i$ is the strain ±1. The coefficient $1/8$ in Eq. (S6) is the probability that the specific line $\boldsymbol{r}_j$ ($\neq \boldsymbol{r}_i$) is chosen as the position of the daughter cell. It is simply replaced with $1/2$ for in-line replications. Similarly, for killing processes, we obtain

$$P^{\pm,\mathrm{kill}}_{j\to i} = \frac{1\pm\phi_j}{2}\frac{1}{8}\frac{1\mp\phi_i}{2}G^{\pm}_i, \qquad (j\neq i) \qquad P^{\pm,\mathrm{kill}}_{i\to i} = \frac{1\pm\phi_i}{2}\frac{1}{2}\frac{1\mp\phi_i}{2}G^{\pm}_i, \tag{S8}$$

where $G_i^{\pm}$ is the probability that a cell of strain ± 1 self-replicates to fill the void generated by killing. It is given by

$$G_i^{\pm} = (1-p_{\rm m})\left(\frac{1}{2}\frac{1\pm\phi_i}{2} + \sum_{j'\in\{\text{n.n. of } i\}}\frac{1}{8}\frac{1\pm\phi_{j'}}{2}\right) + p_{\rm m}\left(\frac{1}{2}\frac{1\mp\phi_i}{2} + \sum_{j'\in\{\text{n.n. of } i\}}\frac{1}{8}\frac{1\mp\phi_{j'}}{2}\right). \tag{S9}$$

A. The case without mutation and killing (self-replication only)

Let us first consider the simplest case without mutation and killing ($p_{\rm m} = 0$ and $\sigma' = 0$), in which we found characteristic coarsening of the two-dimensional voter model in the main article. From Eqs. (S4)-(S7), we obtain

$$\mathrm{E}[\Delta\phi_{j\to i}] = \frac{1}{8}(\phi_j - \phi_i)\sigma\Delta t, \qquad \mathrm{Var}[\Delta\phi_{j\to i}] = \frac{1}{4}(1-\phi_j\phi_i)\left(\frac{\sigma\Delta t}{L_x}\right), \qquad (j\neq i) \tag{S10}$$

and

$$\mathrm{E}[\Delta\phi_{i\to i}] = 0, \qquad \mathrm{Var}[\Delta\phi_{i\to i}] = (1-\phi_i^2)\left(\frac{\sigma\Delta t}{L_x}\right). \tag{S11}$$

Therefore, by Eqs. (S1) and (S2), we have

$$\Delta\phi_i = \frac{1}{8}\sigma\Delta t\sum_{j\in\{\text{n.n. of } i\}}(\phi_j-\phi_i) + \sum_{j\in\{\text{n.n. of } i\}}\sqrt{\frac{\sigma\Delta t}{4L_x}(1-\phi_j\phi_i)}\epsilon_{j\to i}(t) + \sqrt{\frac{\sigma\Delta t}{L_x}(1-\phi_i^2)}\epsilon_{i\to i}(t). \tag{S12}$$

This can be rewritten as

$$\frac{\Delta\phi_i}{\Delta t} = \frac{\sigma}{8}\sum_{j\in\{\text{n.n. of } i\}}(\phi_j-\phi_i) + \sqrt{\frac{\sigma}{4L_x\Delta t}\left\{\sum_{j\in\{\text{n.n. of } i\}}(1-\phi_j\phi_i) + 4(1-\phi_i^2)\right\}}\epsilon_i(t), \tag{S13}$$

where $\epsilon_i(t)$ is white Gaussian noise with $\langle\epsilon_i(t)\rangle = 0$ and $\langle\epsilon_i(t)\epsilon_{i'}(t')\rangle = \delta_{ii'}\delta_{tt'}$. Note that the first term of the right-hand side of Eq. (S13) is a discrete Laplacian.

Now we coarse-grain the description, by replacing the discrete coordinates $\boldsymbol{r}_i$ with continuous ones $\boldsymbol{r}$ and differences with derivatives, and take the limit $\Delta t\to 0$. With the lattice constant a, we obtain

$$\partial_t\phi(\boldsymbol{r},t) = \frac{a^2\sigma}{8}\nabla^2\phi + \sqrt{\frac{2a^2\sigma}{L_x}(1-\phi^2)}\eta(\boldsymbol{r},t), \tag{S14}$$

with $\eta(\boldsymbol{r},t)$ white Gaussian noise in continuous space and time, which satisfies $\langle\eta(\boldsymbol{r},t)\rangle = 0$ and $\langle\eta(\boldsymbol{r},t)\eta(\boldsymbol{r}',t')\rangle = \delta(\boldsymbol{r}'-\boldsymbol{r})\delta(t-t')$. Here we used the relationship $\eta(\boldsymbol{r},t)\simeq\epsilon_i(t)/\sqrt{a^2\Delta t}$ that ensures

$$\int \mathrm{d}\boldsymbol{r}\int \mathrm{d}t\,\langle\eta(\boldsymbol{r},t)\eta(\boldsymbol{r'},t')\rangle = 1. \tag{S15}$$

Importantly, the obtained equation (S14) is exactly the Langevin description of the voter model, proposed by earlier studies [37, 38]. This underpins our numerical observation of the voter-type coarsening presented in Fig. 3.

B. The general case with mutation and killing

For the general case with arbitrary $p_{\rm m}$ and σ', we obtain

$$\begin{aligned}\mathrm{E}[\Delta\phi_{j\to i}] &= \frac{\sigma\Delta t}{8}(1-p_{\rm m})(\phi_j-\phi_i) + \frac{\sigma'\Delta t}{16}(\phi_j-\phi_i)\\ &\quad + \frac{\sigma'\Delta t}{32}(1-2p_{\rm m})(1-\phi_j\phi_i)\left(\phi_i + \sum_{j'\in\{\text{n.n. of } i\}}\frac{\phi_{j'}}{4}\right) - \frac{\sigma\Delta t}{8}p_{\rm m}(\phi_j+\phi_i), \qquad (j\neq i)\end{aligned} \tag{S16}$$

$$\begin{aligned}\mathrm{Var}[\Delta\phi_{j\to i}] &= \frac{1}{4}\frac{\sigma\Delta t}{L_x}(1-p_{\rm m})(1-\phi_j\phi_i) + \frac{1}{8}\frac{\sigma'\Delta t}{L_x}(1-\phi_j\phi_i) + \frac{1}{4}\frac{\sigma\Delta t}{L_x}p_{\rm m}(1+\phi_j\phi_i)\\ &\quad + \frac{1}{16}\frac{\sigma'\Delta t}{L_x}(1-2p_m)(\phi_j-\phi_i)\left(\phi_i + \sum_{j'\in\{\text{n.n. of } i\}}\frac{\phi_{j'}}{4}\right), \qquad (j\neq i)\end{aligned} \tag{S17}$$

and

$$\mathrm{E}[\Delta\phi_{i\to i}] = \frac{\sigma'\Delta t}{8}(1-2p_{\mathrm{m}})(1-\phi_i^2)\left(\phi_i + \sum_{j'\in\{\text{n.n. of } i\}} \frac{\phi_{j'}}{4}\right) - \sigma\Delta t p_{\mathrm{m}}\phi_i, \tag{S18}$$

$$\mathrm{Var}[\Delta\phi_{i\to i}] = \frac{\sigma\Delta t}{L_x}(1-p_{\mathrm{m}})(1-\phi_i^2) + \frac{1}{2}\frac{\sigma'\Delta t}{L_x}(1-\phi_i^2) + \frac{\sigma\Delta t}{L_x}p_{\mathrm{m}}(1+\phi_i^2). \tag{S19}$$

$$\tag{S20}$$

Combining Eqs. (S1) and (S2), we obtain

$$\begin{aligned}\frac{\Delta\phi_i}{\Delta t} = {} & \frac{\sigma'\Delta t}{8}(1-2p_{\mathrm{m}})\left(1-\phi_i^2 + \sum_{j\in\{\text{n.n. of } i\}}\frac{1-\phi_j\phi_i}{4}\right)\left(\phi_i + \sum_{j\in\{\text{n.n. of } i\}}\frac{\phi_j}{4}\right) - \sigma p_m\left(\phi_i + \sum_{j\in\{\text{n.n. of } i\}}\frac{\phi_j+\phi_i}{8}\right) \\ & + \left\{\frac{\sigma}{8}(1-p_{\mathrm{m}}) + \frac{\sigma'}{16}\right\}\sum_{j\in\{\text{n.n. of } i\}}(\phi_j-\phi_i) + \sqrt{\mathrm{Var}[\Delta\phi_{i\to i}] + \sum_{j\in\{\text{n.n. of } i\}}\mathrm{Var}[\Delta\phi_{j\to i}]}\,\epsilon_i(t).\end{aligned} \tag{S21}$$

Then, carrying out the same coarse-graining and the continuous-time limit as in the previous section, we finally arrive at Eq. (6) in the main article:

$$\begin{aligned}\partial_t\phi(\boldsymbol{r},t) = {} & -\frac{\delta F(\phi)}{\delta\phi} + a^2\left[\frac{\sigma}{8}(1-p_{\mathrm{m}}) + \frac{\sigma'}{16}\right]\nabla^2\phi \\ & + \sqrt{\frac{a^2}{L_x}\left[(2\sigma+\sigma')(1-\phi^2) + 2\sigma p_{\mathrm{m}}\phi^2\right]}\,\eta(\boldsymbol{r},t)\end{aligned} \tag{S22}$$

with

$$F(\phi) = -\left(\frac{1-2p_{\mathrm{m}}}{4}\sigma' - p_{\mathrm{m}}\sigma\right)\phi^2 + \frac{1-2p_{\mathrm{m}}}{8}\sigma'\phi^4. \tag{S23}$$

II. SUPPLEMENTAL FIGURES

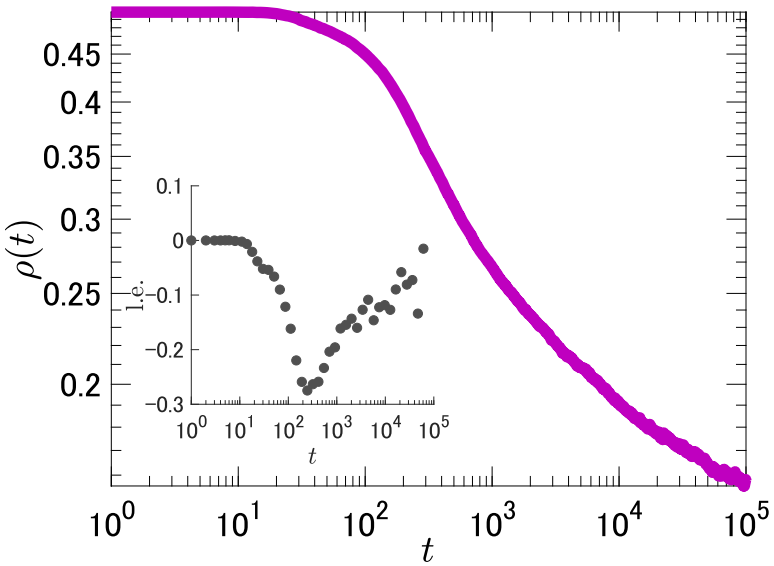

FIG. S1. Decay of the interface density $\rho(t)$ for the model with self-replication only, starting from unbiased random initial conditions. Inset: the local exponent (l.e.) $\mathrm{d}(\ln \rho(t))/\mathrm{d}(\ln t)$. The absence of a plateau region indicates that $\rho(t)$ does not decay by a power law. The value of the local exponent tends to zero asymptotically, being consistent with the logarithmic decay evidenced in Fig. 3(a).

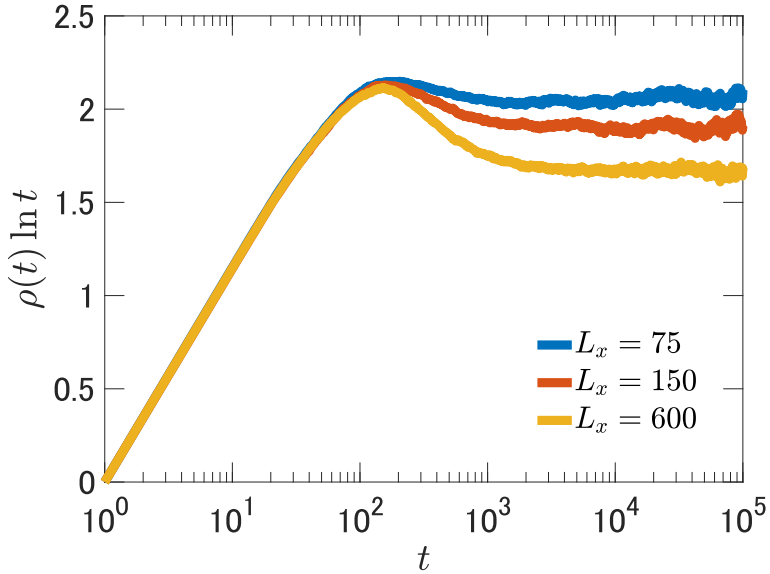

FIG. S2. Channel length (L_x) dependence of the interface density $\rho(t)$, for the model with self-replication only. Each data set is averaged over 10 independent realizations. The size of the cross section is fixed at $L_y = L_z = 150$. Although the asymptotic value of $\rho(t)\ln t$ depends on L_x, the logarithmic decay of $\rho(t)$ is robust against changes in the channel aspect ratio.

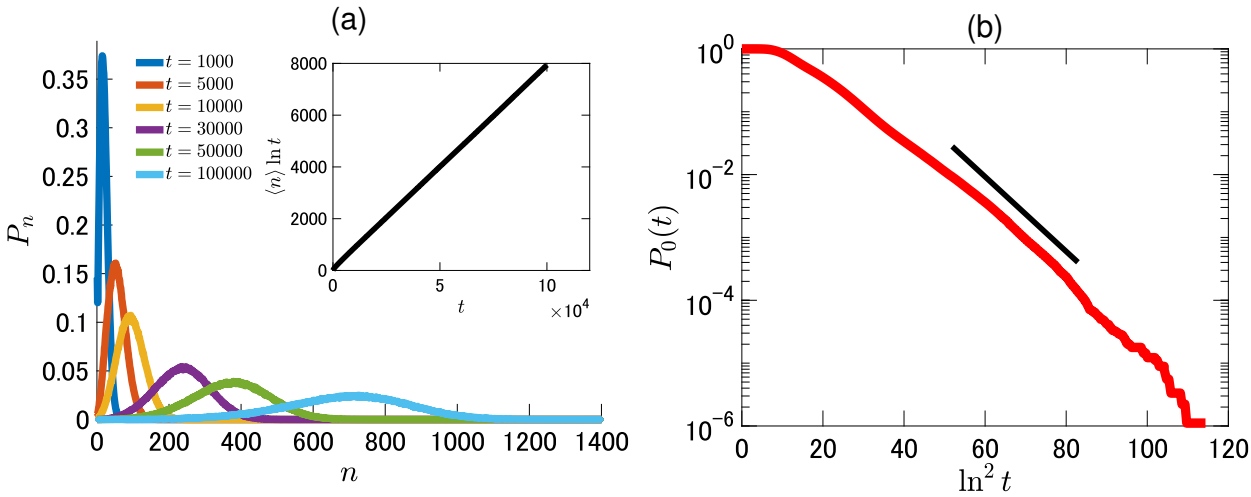

FIG. S3. Persistence properties of $\phi(y, z, t)$, for the model with self-replication only. Each data set is averaged over 10 independent realizations. The system size is $L_x = L_y = L_z = 300$. (a) The main panel shows the probability that $\mathrm{sign}[\phi(y, z, t)]$ changes n times until time t, $P_n(t)$. The inset shows how the average number of sign flips, $\langle n \rangle$ (averaged in space and over realizations), increases with t. Our observation is in agreement with the result for the voter model, $\langle n \rangle \sim t/\ln t$ [32]. (b) Persistence probability $P_0(t)$, i.e., the probability that $\mathrm{sign}[\phi(y, z, t)]$ never changes until time t. We find behavior consistent with the result for the voter model [32], $P_0(t) \sim \exp(-\mathrm{const.} \times \ln^2 t)$, indicated by the solid line.

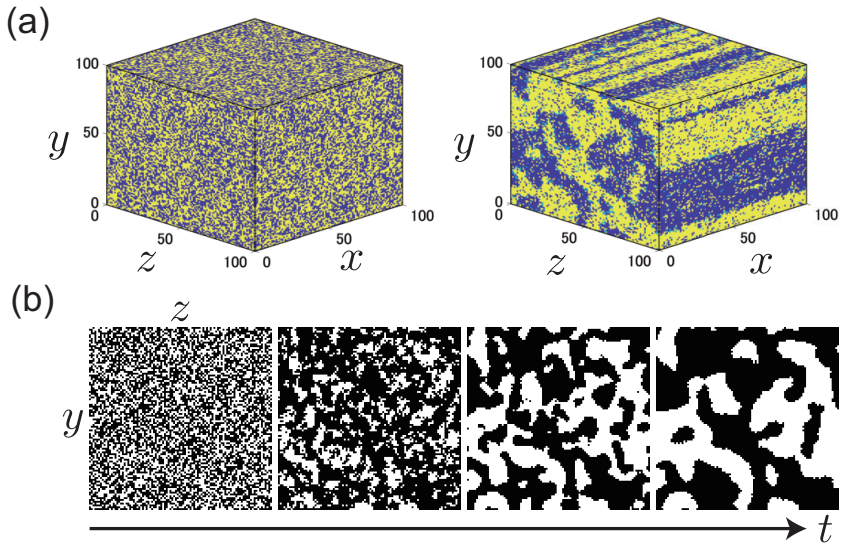

FIG. S4. Evolution of the model with mutation and killing, in the monopolistic phase where killing processes are dominant ($p_{\mathrm{m}} = 0.3$, $C_{\mathrm{k}} = 2.0$). The system size is $L_x = L_y = L_z = 100$. (a) Three-dimensional view of the system. There exist only few voids generated by killing (light blue). The left and right figures show the configuration at different times, $t = 0$ (initial condition) and $t = 5000$, respectively. See also Movie S3. (b) Time evolution of the two-dimensional magnetization field $\phi(y, z, t)$, at $t = 0, 500, 1500, 5000$ from left to right, for the realization shown in (a). Compared with the voter-type, critical coarsening in Fig. 2, coarsening in the monopolistic phase proceeds much faster (notice the different times used in (a)), and the domain interfaces are smoother.

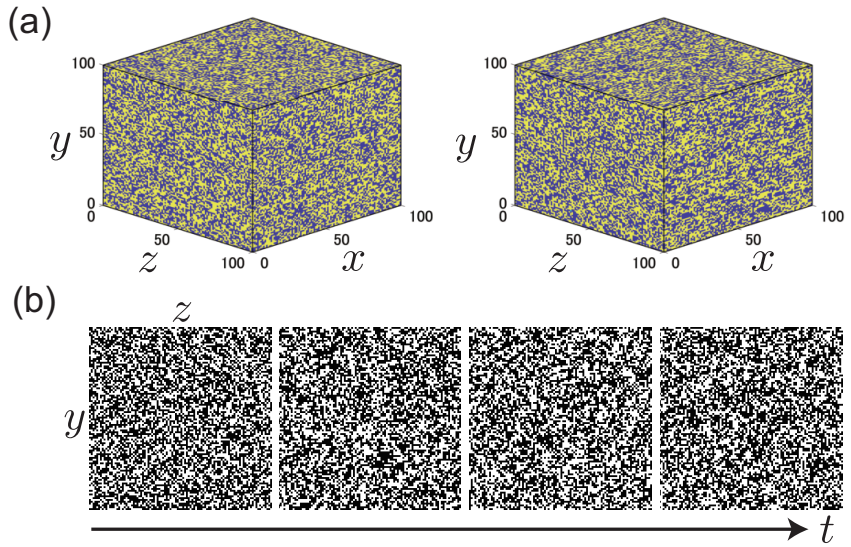

FIG. S5. Evolution of the model with mutation and killing, in the mixed phase where mutation is dominant ($p_{\rm m} = 0.3$, $C_{\rm k} = 0.05$). The system size is $L_x = L_y = L_z = 100$. (a) Three-dimensional view of the system. There exist only few voids generated by killing (light blue). The left and right figures show the configuration at different times, $t = 0$ (initial condition) and $t = 5000$, respectively. See also Movie S4. (b) Time evolution of the two-dimensional magnetization field $\phi(y, z, t)$, at $t = 0, 500, 1500, 5000$ from left to right, for the realization shown in (a). The system remains disordered.

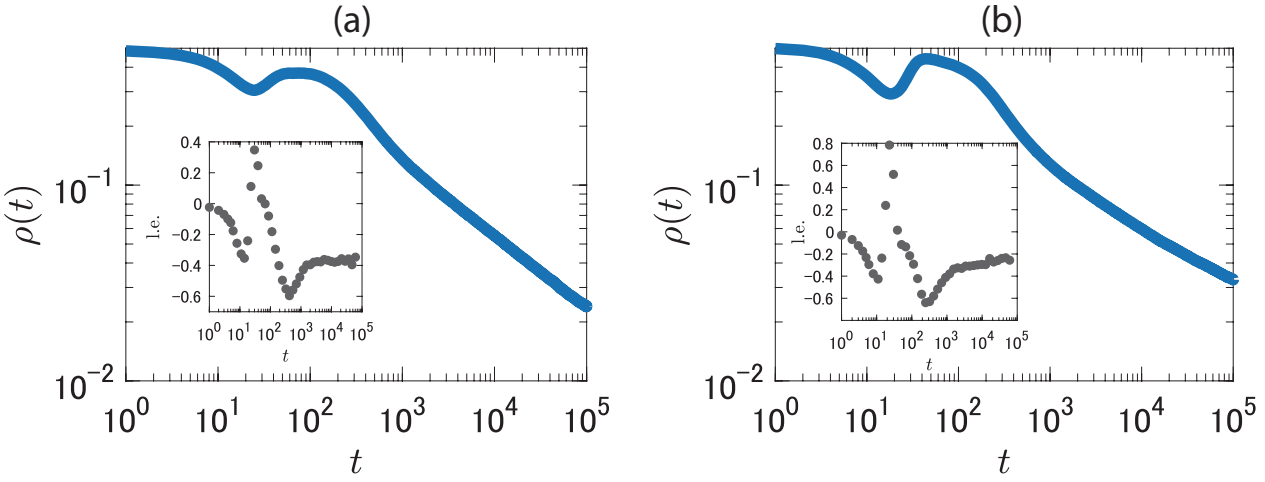

FIG. S6. Decay of the interface density $\rho(t)$ in the presence of killing but without mutation (specifically, $p_{\rm m} = 0, C_{\rm k} = 1$; 10 independent realizations were used). The system size is $L_x = 20$, $L_y = L_z = 200$ for (a) and $L_x = 100, L_y = L_z = 200$ for (b). The insets show the local exponent $\mathrm{d}(\ln \rho(t))/\mathrm{d}(\ln t)$. Although the data suggest power-law decay instead of the logarithmic one found in the critical case, the exponent takes values significantly smaller (in the absolute value) than that of the Ising model with Glauber dynamics, -0.5. The exponent value becomes even smaller for the longer channel.

III. SUPPLEMENTAL MOVIE DESCRIPTIONS

Movie S1:

Time evolution of the model with self-replication only. The left surface is the channel outlet, while the top and right surfaces are the boundaries. The two strains are indicated by yellow and purple. The system size is $L_x = L_y = L_z = 100$. See also Fig. 2.

Movie S2:

Time evolution of the two-dimensional magnetization field $\phi(y, z, t)$ ($\blacksquare$:$\phi > 0$, $\square$:$\phi \leq 0$), for the model with self-replication only. The system size is $L_x = L_y = L_z = 200$.

Movie S3:

Time evolution of the model with mutation and killing, in the monopolistic phase ($p_{\mathrm{m}} = 0.3,\ C_{\mathrm{k}} = 2.0$). The left surface is the channel outlet, while the top and right surfaces are the boundaries. The two strains are indicated by yellow and purple. The system size is $L_x = L_y = L_z = 100$. See also Fig. S4.

Movie S4:

Time evolution of the model with mutation and killing, in the mixed phase ($p_{\mathrm{m}} = 0.3,\ C_{\mathrm{k}} = 0.05$). The left surface is the channel outlet, while the top and right surfaces are the boundaries. The two strains are indicated by yellow and purple. The system size is $L_x = L_y = L_z = 100$. See also Fig. S5.